JOURNAL OF OPTOELECTRONICS AND ADVANCED MATERIALS Vol. 8, No. 2, April 2006, p. 731 - 736

Section 8. Miscellaneous materials

Crystal field studies of the $MgAl_2O_4 : Ni^{2+}$ ground and excited state absorption

M. G. BRIK[a,b], N. M. AVRAM[*c], C. N. AVRAM[c]
[a]*Fukui Institute for Fundamental Chemistry, Kyoto University, 34-4 Takano Nishihiraki-cho, Sakyo-ku, Kyoto, 606-8103, Japan*
[b]*School of Science and Technology, Kwansei Gakuin University, 2-1 Gakuen, Sanda, Hyogo 669-1337, Japan*
[c]*Department of Physics, West University of Timisoara, Bd. V. Parvan No. 4, 300223, Timisoara, Romania*

The exchange charge model of crystal field theory has been used to analyze the ground and excited state absorption of octahedrally coordinated Ni^{2+} ion in $MgAl_2O_4$. The parameters of the crystal field acting on the Ni^{2+} ion are calculated from the crystal structure data. The obtained energy level schemes were compared with experimental ground and excited state absorption spectra; a good agreement with experimental data is demonstrated. From the analysis of the experimental spectra, the Stokes shift, the effective phonon energy and the zero-phonon line position all were evaluated.

(Received January 18, 2006; accepted March 23, 2006)

Keywords: Crystal field theory, 3d-ions, Ground and excited state absorption

1. Introduction

Ni^{2+}-doped crystals exhibit broad absorption bands in the visible and infrared spectral range [1]. As a rule, divalent nickel enters octahedral sites in the crystals, though in some garnets like $Gd_3Ga_5O_{12}$ [1, 2] and $Ca_3Sc_2Ge_3O_{12}$ [3] tetrahedrally coordinated Ni^{2+} ions were detected as well resulting in more complicated spectra due to the overlap of the absorption bands arising from different centers. The emission lifetime of octahedral Ni^{2+} ions is of the order of ms [1] and from the point of view of the potential laser application the Ni^{2+}-doped crystals seem to be very attractive. With this aim in view, $Y_3Al_5O_{12}:Ni^{2+}$ and $Gd_3Sc_2Ga_3O_{12}:Ni^{2+}$ have been proposed in [4] as promising materials for solid-state lasers. However, no laser oscillation was obtained at room temperature so far [1], and the main reason is due to a strong excited state absorption (ESA), which overlaps with the fluorescence band. The ESA measurements from the $^3T_2$ (^3F) first excited state of Ni^{2+} in various crystals (MgO, MgF_2, $Gd_3Ga_5O_{12}$) were reported in [5–7].

Among other Ni^{2+}-doped crystals, spinel $MgAl_2O_4$ was reported in [8, 9], and ESA studies of $MgAl_2O_4:Ni^{2+}$ were performed in [10]. In the present paper we analyze both ground state absorption (GSA) and ESA of $MgAl_2O_4:Ni^{2+}$ using the exchange charge model (ECM) [11] of crystal field. We calculate the crystal field parameters using the crystal structure data [12], compute the crystal field splitting of the Ni^{2+} terms using only one fitting parameter of the ECM, and determine the Stokes shift, the effective phonon frequency and the zero-phonon line energy from the experimental absorption and emission spectra [10].

2. Spectroscopic and crystal structure data for $MgAl_2O_4:Ni^{2+}$

According to [12] $MgAl_2O_4$ belongs to the Fd-3m space group with lattice constant $a = 8.0806$ Å. After doping, Ni^{2+} ions substitute for Al^{3+} at the octahedral sites. Experimental measurements of the GSA and ESA in [10] revealed three strong broad absorption bands at 970 nm, 595 nm, and 365 nm which were unambiguously ascribed to the spin-allowed transitions from the $^3A_2$ (^3F) ground state to the orbital triplets $^3T_2$ (^3F), $^3T_1$ (^3F), and $^3T_1$ (^3P), respectively. Two additional small peaks in the GSA spectrum at 770 nm and 430 nm were assigned to the spin-forbidden transitions to the ^1E (^1D) and $^1T_2$ (^1D) levels. From the experimental positions of these bands, the authors of Ref. [10] estimated the values of the Racah parameters *B*, *C*, and crystal field strength *Dq* to be (in cm^{-1}): 865, 3254, and 1040. A small ratio $Dq/B = 1.2$ indicates the weak crystal field case is realized in the considered host. The emission spectrum exhibits one broad band with a peak at around 1180 nm, and it is due to the $^3T_2$ (^3F) $\rightarrow$ $^3A_2$ (^3F) transition. Both absorption and emission bands appear structureless; in addition, no zero-phonon lines were detected either in emission or in absorption spectra. These facts serve as an experimental proof for strong electron-vibronic coupling in the considered material. Detailed ESA measurements performed in [10] at room temperature lead to the detection of three broad absorption bands centered at about 1700 nm, 750 nm, and 580 nm. The first band was ascribed to the $^3T_2$ (^3F) $\rightarrow$ $^3T_1$ (^3F) transition; the second and the third – to the $^3T_2$ (^3F) $\rightarrow$ $^1T_1$ (^1D) and $^3T_2$ (^3F) $\rightarrow$ $^3T_1$ (^3P), respectively.

In the next sections these experimental results will be confirmed by detailed crystal field calculations.

3. Crystal field calculations for $MgAl_2O_4:Ni^{2+}$

Energy levels of the Ni^{2+} ion in this work are represented by the eigenvalues of the following crystal field Hamiltonian [11]:

$$H = \sum_{p=2,4} \sum_{k=-p}^{p} B_p^k O_p^k , \quad (1)$$

where O_p^k are the linear combinations of irreducible tensor operators acting on angular parts of the Ni^{2+} ion wave functions, and B_p^k are crystal field parameters containing all information about geometrical structure of an impurity center. As formulated in [11], these parameters can be written as a sum of two terms:

$$B_p^k = B_{p,q}^k + B_{p,S}^k . \quad (2)$$

The first contribution is due to the electrostatic interaction between optical electrons of an impurity ion and ions of crystal lattice (treated at point charges, without taking into account their electron structure), and the second one is proportional to the overlap of the wave functions of an impurity ion and ligands. In other words, this term includes all effects of the covalent bond formation and exchange interaction. Inclusion of these effects significantly improves an agreement between calculated and experimentally observed energy levels. Expressions for calculating both contributions to the crystal field parameters in the case of 3*d*-ion are as follows [11]:

$$B_{p,q}^k = -K_p^k e^2 \left\langle r^p \right\rangle \sum_i q_i \frac{V_p^k(\theta(i),\varphi(i))}{R(i)^{p+1}}, \quad (3)$$

$$B_{p,S}^k = K_p^k e^2 \frac{2(2p+1)}{5} \sum_i \left(G_s S_s(i)^2 + G_\sigma S_\sigma(i)^2 + \gamma_p G_\pi S_\pi(i)^2 \right) \frac{V_p^k(\theta(i),\varphi(i))}{R(i)} . \quad (4)$$

The sums are carried out over lattice ions denoted by *i* with charges q_i; $R(i),\theta(i),\varphi(i)$ are the spherical coordinates of the *i*-th ion of crystal lattice in the system of reference centered at the impurity ion. The averaged values $\left\langle r^p \right\rangle$ of *p*-th power of the impurity ion electron radial coordinate can be found in Ref. [13]. The values of the numerical factors K_p^k, γ_p and expressions for the polynomials V_p^k are given in [11]. The overlap integrals between *d*-functions of the central ion and *p*- and *s*-functions of the ligands are denoted by S_s, S_σ, S_π (they correspond to the following integrals (in $\langle lm|l'm'\rangle$ notation): $S_s = \langle d0|s0\rangle, S_\sigma = \langle d0|p0\rangle, S_\pi = \langle d1|p1\rangle$) . G_s, G_σ, G_π are dimensionless adjustable parameters of the model, which are determined from the positions of the first three absorption bands. For practical purposes, it is sufficient to assume them be equal to each other: $G_s = G_\sigma = G_\pi = G$ (in this case only the first absorption band is required to determine the value of G), and in this paper we use this simplified model. The strong advantage of the ECM is that if the *G* parameter is determined to fit the first absorption band, the other energy levels, located higher in energy, will also fit experimental spectra fairly well.

The ECM has been successfully applied for the calculations of the energy levels of both rare earth [11,14–17] and transition metal ions in different hosts as well [18–23] and analysis of the electron-phonon coupling and non-radiative transitions [24–26].

Since the second rank point charges parameters $B_{2,q}^k$ decrease not so fast as the fourth rank parameters $B_{4,q}^k$ (as $1/R^3$ and $1/R^5$, respectively), the contribution of the ligands from the second and further coordination spheres can be quite significant. To increase accuracy in calculating the point charge contribution to the crystal field parameters, we considered large cluster consisting of 791 ions, namely 1 Ni^{2+}, 223 Al^{3+}, 123 Mg^{2+}, and 444 O^{2-}. This cluster enables to take into account the contribution of ions located at the distances up to 15.117 Å. For the exchange charge parameters (Eq. (4)) only the nearest ligands were taken into account, since the overlap between an impurity ion and ligands from other than the first coordination sphere can be safely neglected. The overlap integrals between the Ni^{2+} and O^{2-} ions needed for calculating the exchange charge contribution $B_{p,S}^k$ to the crystal field parameters were computed numerically using the radial wave functions of the Ni^{2+} ion given in [27] and O^{2-} ion given in [28]. The dependence of the overlap integrals on the interionic distance *r* (in atomic units; $3.3 < r < 4.3$) is given by the following exponential approximations:

$$S_s = \langle d0|s0\rangle = -0.71284\exp(-0.66179r) , \quad (5)$$

$$S_\sigma = \langle d0|p0\rangle = 0.84696\exp(-0.68325r) , \quad (6)$$

$$S_\pi = \langle d1|p1\rangle = 1.13280\exp(-0.86486r) . \quad (7)$$

Using Eqs. (1) – (4), crystal structure data from [12], and exponential approximations of the $Ni^{2+} - O^{2-}$ overlap integrals from Eqs. (5) – (7), we obtained the values of the crystal field parameters, which are given in Table 1. The point and exchange charges contributions are shown separately to stress out an importance of the overlap effects and their influence on the crystal field parameters values. The crystal field Hamiltonian (1) was diagonalized in the space of 25 wave functions of the spin-triplet terms ^{3}F, ^{3}P and the spin-singlet terms ^{1}S, ^{1}D, ^{1}G of the Ni^{2+} ion. The Racah parameters *B* and *C* which define the energy separation between the above terms were chosen to be (in cm^{-1}): 865 and 3254, respectively [10]. This parameters are reduced with respect to those for a free Ni^{2+} ion ($B = 1068$ cm^{-1}, $C = 4457$ cm^{-1} [29]) due to the covalent effects. Such a reduction serves as a firm justification of application of the ECM for the considered case. The adjustable parameter *G* was defined by fitting the calculated splittings to the experimental ones, and turned out to be 0.375. Finally, the obtained energy levels are listed in Table 2, in comparison with experimental measurements [10].

Table 1. Crystal field parameters (in cm^{-1}) of octahedral Ni^{2+} in $MgAl_2O_4$.

Parameter	Point charges contribution	Exchange charges contribution	Total value
B_2^{-2}	– 211	– 831	– 1042
B_2^{-1}	808	– 1663	– 855
B_2^0	– 15	0	– 15
B_2^1	– 808	1663	855
B_2^2	0	0	0
B_4^{-4}	0	0	0
B_4^{-3}	117	1592	1709
B_4^{-2}	33	455	488
B_4^{-1}	– 17	– 227	– 244
B_4^0	882	1821	2703
B_4^1	17	227	244
B_4^2	0	0	0
B_4^3	117	1592	1709
B_4^4	4410	9103	13513

Fig. 1 shows the Tanabe-Sugano diagram [30] for Ni^{2+} in octahedral environment calculated for the used in the calculations values of the Racah parameters. For the convenience, the spin-triplet states are shown by solid lines, the spin-singlet states – by crosses. The ratio Dq/B = 1.19, which corresponds to $MgAl_2O_4$:Ni^{2+} is shown by a vertical line.

Since the absorption bands of the Ni^{2+} ion are very broad [10], we calculated the averaged values of energy for the groups of states, arising from the orbitally degenerated states after they are split by the low-symmetry component of crystal field. As seen from Table 1, there exists very good correspondence between positions of the calculated energy levels and observed in GSA experiments.

From the averaged position of the $^3T_2$ (^3F) energy level we estimated the crystal field strength Dq to be equal to 1031 cm^{-1} for $MgAl_2O_4$, what is in a favorable agreement with the results of Ref. [10] (1040 cm^{-1}).

Comparison between the energies for the ESA transitions from the calculated energy level scheme and experimental results is shown in Table 3. Again, the averaged energies for all transitions were found and compared to their experimental counterparts. Again, the correspondence is satisfactory good, since the ESA bands were also very broad.

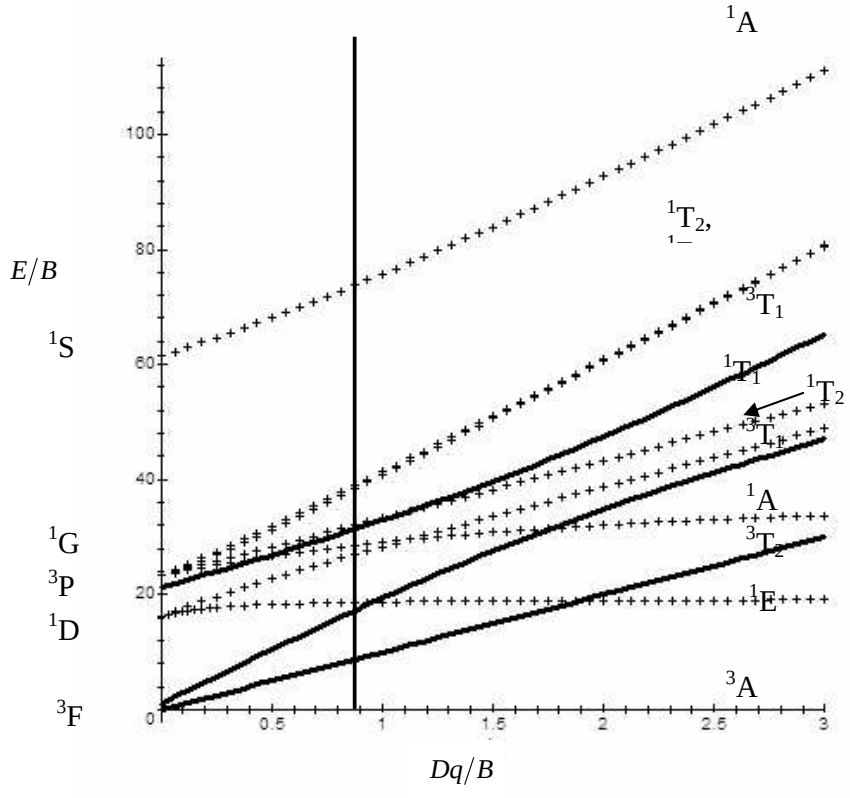

Fig. 1. The Tanabe-Sugano diagram for a $3d^8$ ion in an ideal octahedral field. C/B = 3.76. The vertical line corresponds to the position of Ni^{2+} ion in $MgAl_2O_4$.

Table 2. Positions of energy levels (in cm^{-1}) of octahedral Ni^{2+} in $MgAl_2O_4$.

O_h irrep. Repress.	Calculated (this work)		Experimental values (GSA,[10])
	Averaged		
$^3A_2$ (^3F)	0	0	0
	10251		
$^3T_2$ (^3F)	10290	10310	10309
	10390		
^1E (^1D)	13099		12987
	15997		
$^3T_1$ (^3F)	16898	16622	16807
	16971		
$^1A_1$ (^1G)	21857		
	22809		
$^1T_2$ (^1D)	22967	23013	23256
	23263		
	26783		
$^3T_1$ (^3P)	27169	27299	27397
	27945		
	27137		
$^1T_1$ (^1G)	27181	27195	
	27268		
	35180		
$^1T_2$ (^1G)	35342	35237	
	35458		
^1E (^1G)	35855	35888	
	35920		
$^1A_1$ (^1S)	57364		

Table 3. ESA transitions (in cm^{-1}) of octahedral Ni^{2+} in $MgAl_2O_4$.

Transitions from the lowest $^3T_2$ (^3F) level to:	Calculated (this work)		Experimental values (ESA,[10])
	Averaged		
$^3T_1$ (^3F)	5746	6371	Peak at 5882 cm^{-1}, a broad band from 4762 cm^{-1} to 1150 nm 8696 cm^{-1}
	6647		
	6720		
$^1T_2$ (^1D)	12558	12762	13333
	12716		
	13012		
$^3T_1$ (^3P)	16532	17048	17241
	16918		
	17694		

4. Electron-phonon coupling in $MgAl_2O_4:Ni^{2+}$ and emission band shape modeling

Following the authors of Ref. [10], the system in question is referred to as exhibiting a strong electron-phonon coupling. In this section we estimate the value of Stoks shift *S* and effective phonon energy, employing a single-coordinate configurational model in harmonic approximation [31]. The two main parameters which describe the electron-phonon coupling are the Huang-Rhys parameter *S* and the effective phonon energy $\hbar\omega$. The former is defined as the number of phonons of the energy $\hbar\omega$ excited in the absorption transition [31]:

$$S = \frac{E_{dis}}{\hbar\omega} \tag{8}$$

where E_{dis} is defined in Fig. 2. *S* and $\hbar\omega$ are related to the difference between the first absorption and corresponding emission bands peaks ΔE by the following expression [31–33]:

$$\Delta E = (2S-1)\hbar\omega. \tag{9}$$

The second equation which is required for to calculate the values of *S* and $\hbar\omega$ is [31]:

$$\Gamma(T) = 2.35\hbar\omega\sqrt{S\coth\left(\frac{\hbar\omega}{2kT}\right)}, \tag{10}$$

where $\Gamma(T)$ is the full width at half maximum (FWHM) of the emission band at the absolute temperature *T*. In order to solve the equations (9) and (10) we used the spectroscopic data from [10]. According to these data, the energetical Stokes shift ΔE is about 1835 cm^{-1}, and the FWHM of the $^3T_2 \rightarrow {}^3A_2$ emission band at 4.2 K is about 1037 cm^{-1}. Solving Eqs. (9) and (10) yields S = 5.28, $\hbar\omega$ = 192 cm^{-1}. Indeed, the value of *S* is rather large (for example, for Cr^{4+} ions, whose electron configuration is d^2 has the same LS terms as the d^8 configuration of Ni^{2+}) this value is about 2 in various compounds [1]), thus confirming the conclusion about strong electron-phonon coupling in the system in question [10]. The Ni^{2+} $^3T_2 \rightarrow {}^3A_2$ emission lifetime was shown in [10] to increase from 0.4 ms at room temperature to 1.5 ms at 77 K. This change is not so significant, as, for example, in $Y_3Al_5O_{12}:Cr^{4+}$, where the Cr^{4+} emission lifetimes at room temperature and 0 K differ by the order of magnitude [34]. Therefore, the role of the non-radiative relaxation in $MgAl_2O_4:Ni^{2+}$ is not so important, and this can be explained by low effective phonon energy $\hbar\omega$. It is less than 200 cm^{-1}, whereas, for example, for $Sc_2O_3:Cr^{3+}$it is 499 cm^{-1} [20], for $Y_3Al_5O_{12}:Cr^{4+}$ it is 400 cm^{-1} [34]. A small value of the effective phonon energy implies a large number of the phonons bridging the gap between the ground and first excited states (more than 40) in the studied system, and this leads to a small value of the non-radiative transition probability and, as a consequence, a weak thermal dependence of the emission lifetime.

The zero-phonon line was not observed in [10], but its position can be estimated by means of the emission band shape modeling. The shape of the broad band can be reproduced by the envelope of the lines given by the equation [31,35].

$$I = I_0 \sum_m exp(-S)\frac{S^m}{m!}\delta(E_0 \mp m\hbar\omega - E), \quad (11)$$

where I is the band intensity, E_0 is the zero-phonon energy, E is the photon energy, m is an integer (this is the number of phonons involved into the transition) and all other quantities entering Eq. (11) are defined above. The "–" sign relates to the emission transition, and the "+" sign relates to the absorption transition. The only parameter which has not been defined yet and which is allowed to vary freely is E_0. The best fit of the predicted by Eq. (11) emission band shape with the experimental spectra [10] was obtained with the above defined values of S and $\hbar\omega$ and value of the zero-phonon line energy $E_0 = 9310$ cm^{-1} (Fig. 2).

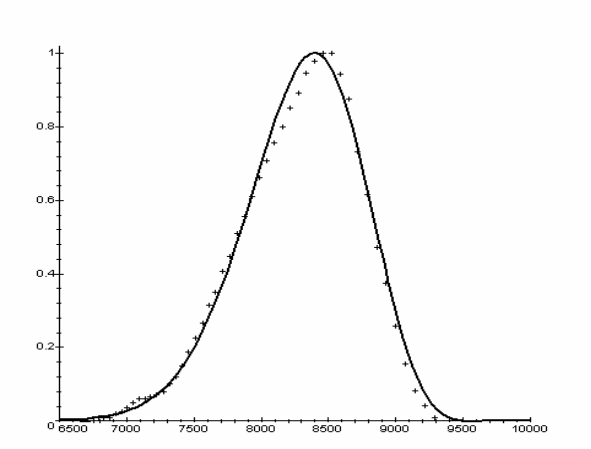

Fig. 2. Theoretical (solid line) and experimental (crosses, [2]) band shapes of the $^3T_2 \rightarrow {}^3A_2$ emission transition in $MgAl_2O_4:Ni^{2+}$.

4. Conclusion

Calculations of the crystal field parameters and energy level structure of the octahedrally coordinated Ni^{2+} ion in $MgAl_2O_4$ were performed in the framework of the exchange charge model of crystal field with one adjustable parameter G, describing the overlap between the wave functions of the central ion and its nearest environment. Results of the energy levels calculations performed in the present paper are in a good agreement with experimental measurements of both GSA and ESA. The exchange charge model with its possibility of explicit inclusion of the overlap integrals into the expression for calculating the crystal field parameters provides an adequate description of the energy levels scheme of the Ni^{2+} in the studied crystal. The Stokes shift $S = 5.28$ and the effective phonon energy $\hbar\omega = 192$ cm^{-1} have been deduced from the experimental spectra of emission and absorption of $MgAl_2O_4:Ni^{2+}$. The Ni^{2+} $^3T_2 \rightarrow {}^3A_2$ emission band shape was calculated using the single configuration coordinate model. Fitting of the calculated bands shapes to the experimental spectra allowed for estimating the zero-phonon energy of the above transition to be 9310 cm^{-1}.

Acknowledgments

M.G. Brik acknowledge the financial support from the Japanese Ministry of Education, Culture, Sports, Science and Technology (MEXT) in a project on Computational Materials Science Unit at Kyoto University.

References

[1] S. Kück, Appl. Phys. **B 72** 515 (2001).
[2] J. Koetke, G. Huber, K. Peterman, J. Lumin**.** **48-49**, 564 (1991).
[3] E. Zannoni, E. Cavalli, A. Toncelli, M. Tonelli, M. Bettinelli, J. Phys. Chem. Solids **60**, 449 (1999).
[4] E. P. Dubrovina, V. A. Sandulenko, M .I. Demchuk, N.V. Kuleshov, and V.P. Mikhailov, Chem. Phys. Lett. **170**, 473(1990).
[5] R. Moncorge, T. Benyattou, Phys. Rev. **B 37**, 9186 (1988).
[6] S. A. Payne, Phys. Rev. **B 41,** 6109 (1990).
[7] J. Koetke, K. Peterman, G. Huber, J. Lumin. **60-61**,197 (1993).
[8] J. F. Donegan, F. J. Bergin, T. J. Glynn, G. F. Imbush, J. P. Remeika, J. Lumin. **35**, 57 (1986) C. Wyon, J. J. Aubert, F. Auzel, J. Cryst. Growth **79,** 710 (1986).
[9] N. V. Kuleshov, V. G. Shcherbitsky, V. P. Mikhailov, S. Kück, J. Koetke, K. Peterman, G. Huber, J. Lumin**.** **71**, 265 (1997).
[10] B. Z. Malkin, in: A. A. Kaplyanskii, B. M. Macfarlane (Eds.), Spectroscopy of solids containing rare-earth ions, North-Holland, Amsterdam, 1987, pp. 33–50.
[11] T. Yamanaka, Y. Takeuchi, M. Tokonami, Acta Cryst. **B 40,** 96 (1984).
[12] A. G. Abragam, B. Bleaney, Electron Paramagnetic Resonance of Transition Ions, Oxford, Clarendon, 1970.
[13] G. A. Bogomolova, L. A. Bumagina, A. A. Kaminskii, B. Z. Malkin, Fizika Tverdogo Tela (Soviet Physics of the Solid State) **19**, 1439 (1977).
[14] M. N. Popova, S. A. Klimin, E. P. Chukalina, R. Z. Levitin, B. V. Mill, B. Z. Malkin, E. Antic-Fidancev, J. Alloys Compds. **380**, 84 (2004).
[15] M. N. Popova, E. P. Chukalina, B. Z. Malkin, A. I. Iskhakova, E. Antic-Fidancev, P. Porcher, J. P. Chaminade, Phys. Rev. **B 63**, 075103 (2001).
[16] M. N. Popova, S. A. Klimin, E. P. Chukalina, E. A. Romanov, B. Z. Malkin, E. Antic-Fidancev, B. V. Mill, G. Dhalenne, Phys. Rev. **B71**, 024414 (2005).
[17] M. G. Brik, C. N. Avram, N. M. Avram, OSA Trends in Optics and Photonics, Vol. 68, Advanced Solid-State Lasers, Martin E. Fermann and Larry R. Marshall, eds. (Optical Society of America, Washington, DC 2002), pp. 275–279.

[18] C. Jousseaume, D. Vivien, A. Kahn-Harari, B. Z. Malkin, Opt. Mater **24**, 143 (2003).
[19] M. G. Brik, N. M. Avram, Z. Naturforsch. **59a,** 799 (2004).
[20] M. G. Brik, C. N. Avram, I. Tanaka, Phys. Status Solidi **B 241**, 2501 (2004).
[21] M. G. Brik, N. M. Avram, C. N. Avram, Sol. State Commun. **132**, 831 (2004).
[22] M. G. Brik, N. M. Avram, C. N. Avram, I. Tanaka, Eur. Phys. J. Appl. Phys. **29**, 239 (2005)
[23] S. I. Klokishner, B. S. Tsukerblat, O. S. Reu, A. V. Palii, S. M. Ostrovsky, Opt. Mater. (2005, article in press).
[24] M. G. Brik, C. N. Avram, J. Lumin. **102-103**, 283(2003).
[25] M. N. Popova, E. P. Chukalina, B. Z. Malkin, S. K. Saikin, Phys. Rev. **B 61**, 7421 (2000).
[26] E. Clementi and C. Roetti, Atomic Data and Nuclear Data Tables **14**, 177 (1974).
[27] M. V. Eremin, in: Spectroscopy of Laser Crystals (in Russian), Moscow, 1989, pp. 30–44.
[28] P. H. M. Uylings, A. J. J. Raassen, J. F. Wart, J. Phys. **B 17**, 4103 (1984).
[29] S. Sugano, Y. Tanabe, H. Kamimura, Multiplets of Transition-Metal Ions in Crystals (Academic Press, New York, 1970).
[30] B. Henderson, G. F. Imbush, Optical Spectroscopy of Inorganic Solids, Clarendon Press, Oxford, 1989.
[31] G. A. Torchia, O. Martinez Matos, P. Vaveliuk, J. O. Tocho, Solid State Commun. **127**, 535 (2003).
[32] G. A. Torchia, O. Martinez-Matos, N. M. Khaidukov, J. O. Tocho, Solid State Commun.**130**, 159 (2004).
[33] H. Eilers, U. Hömmerich, S. M. Jacobsen, W. M. Yen, K. R. Hoffman, W. Jia, Phys. Rev. **B 49**, 15505 (1994).
[34] I. Sokolska, S. Kück, Spectrochim. Acta **A 54**, 1695 (1998).

*Corresponding author: avram@physics.uvt.ro